OPEN

Descemet's Membrane Biomimetic Microtopography Differentiates Human Mesenchymal Stem Cells Into Corneal Endothelial-Like Cells

Angela Gutermuth, MD, PhD, Jessika Maassen, BS,* Emely Harnisch, MD,* Daniel Kuhlen, BS,* Alexis Sauer-Budge,† Claudia Skazik-Voogt, MD, PhD,* and Katrin Engelmann, PhD‡§*

Purpose: Loss of corneal endothelial cells (CECs) bears disastrous consequences for the patient, including corneal clouding and blindness. Corneal transplantation is currently the only therapy for severe corneal disorders. However, the worldwide shortages of corneal donor material generate a strong demand for personalized stem cell–based alternative therapies. Because human mesenchymal stem cells are known to be sensitive to their mechanical environments, we investigated the mechanotransductive potential of Descemet membrane–like microtopography (DLT) to differentiate human mesenchymal stem cells into CEC-like cells.

Methods: Master molds with inverted DLT were produced by 2-photon lithography (2-PL). To measure the mechanotransductive potential of DLT, mesenchymal stem cells were cultivated on silicone or collagen imprints with DLT. Changes in morphology were imaged, and changes in gene expression of CEC typical genes such as zonula occludens (ZO-1), sodium/potassium (Na/K)-ATPase, paired-like homeodomain 2 (PITX2), and collagen 8 (COL-8) were measured with real-time polymerase chain reaction. At least immunofluorescence analysis has been conducted to confirm gene data on the protein level.

Results: Adhesion of MSCs to DLT molded in silicone and particularly in collagen initiates polygonal morphology and monolayer formation and enhances not only transcription of CEC typical genes such as ZO-1, Na/K-ATPase, PITX2, and COL-8 but also expression of the corresponding proteins.

Conclusions: Artificial reproduction of Descemet membrane with respect to topography and similar stiffness offers a potential innovative way to bioengineer a functional CEC monolayer from autologous stem cells.

Key Words: corneal endothelial cell loss, mechanotransduction, mesenchymal stem cells, Descemet topography

(*Cornea* 2019;38:110–119)

The most important function of the corneal endothelium (CE) is maintenance of corneal transparency by regulating water content of the corneal stroma.[1] If the number of corneal endothelial cells (CECs) falls below a certain threshold because of traumatic injury, disease, or normal aging processes, functionality of the CE is decreased, and the cornea swells and becomes milky, leading to eventual vision loss.[2] Despite having high metabolic activity, human CECs (hCECs) do not proliferate in vivo because these cells arrest in the G1 phase of the cell cycle. The mitotic inactivity and the local absence of suitable precursor cells disenable hCECs to repair damage of the endothelial layer.[3]

Currently, the only therapies to restore visual acuity under these conditions are full-thickness corneal transplantation and endothelial keratoplasty.[4] Although the surgical practice is well established, the quality and quantity of corneal donor tissue limits the success of these conventional therapies.[5,6] Thus, there is a strong need for alternative therapies for visual impairment caused by corneal endothelial cell loss. A promising approach is to expand donor hCECs in vitro and transplant the engineered functional monolayer either individually or adhered to a compatible scaffold. Because hCECs rapidly become senescent or undergo endothelial to mesenchymal transitions,[7–9] some research groups investigate the objective to improve the proliferation and adhesion behavior of hCECs[10–14] or transform hCECs into cell lines[15] or to inject hCECs directly. Although these approaches contribute to enhancing the proliferation potential of hCECs, the carcinogenic potential of transformed hCECs or endothelial to mesenchymal transition after passaging of cells in vitro limits the clinical applicability. Recently, Kinoshita et al[16] may have overcome these well-known problems by injecting human CECs supplemented with a ROCK inhibitor and gained thereby an increase of CEC in 11 patients.

Received for publication April 24, 2018; accepted July 27, 2018. Published online ahead of print October 10, 2018.

From the *Department for Applied Cell Biology, Fraunhofer Institute for Production Technology, Aachen, Germany; †Exponent, Department for Polymer Science & Materials Chemistry, Natick, MA; ‡Medical Center for Ophthalmology, Chemnitz, Germany; and §Experimental Ophthalmology, Institute of Anatomy Dresden, Technical University of Dresden, Dresden, Germany.

The authors have no funding or conflicts of interest to disclose.

Data availability: The data sets generated and analyzed during the current study are available from the corresponding author on reasonable request.

Supplemental digital content is available for this article. Direct URL citations appear in the printed text and are provided in the HTML and PDF versions of this article on the journal's Web site (www.corneajrnl.com).

Correspondence: Angela Gutermuth, MD, PhD, Fraunhofer Institute for Production Technology, Steinbachstraße 17, Aachen 52074, Germany (e-mail: angela.gutermuth@ipt.fraunhofer.de).

However, an alternative approach is to use human stem cells as a CEC source. The most closely related stem cells might be the hCEC progenitor cells, which in fact have been isolated by several groups.[17–19] However, these cells acquire altered epigenetic modifications during cultivation, which could in turn inhibit their further proliferation or result in terminal differentiation, followed by senescence.[20] Other highly potent stem cell sources such as embryonic stem cells[21] and induced pluripotent stem cells have the major advantages of pluripotency and an unlimited proliferation capacity. However, ethical concerns, immune rejection, and risk of teratoma formation have limited application of stem cells in clinical trials.[22,23] Apart from pluripotent stem cell sources, adult multipotent mesenchymal stem cells (MSCs) also represent a potential source for hCECs including umbilical cord blood MSCs,[24] bone marrow–derived endothelial progenitor cells,[25] or corneal stromal derived stem cells of neural crest origin.[26,27] In fact, it has been demonstrated that addition of specific biochemical factors from hCECs[28] or human lens epithelial cells (hLECs)[24] induced expression of hCEC typical markers (eg, ZO-1 and N-cadherin) but did not achieve the typical CEC morphology. Because the cytoplasm and nucleus shape have a crucial influence on cell function,[29] we attempted to achieve CEC differentiation by converting the human mesenchymal stem cell (hMSC) typical fibroblastic-like morphology into a polygonal one. To this aim, we reproduced the microstructure of native Descemet membrane and cultured skin-derived hMSCs on these biomimetic structures. The hMSCs expressed hCEC typical markers, changed their morphology to a polygonal shape, started to develop a monolayer configuration, and expressed CEC-specific genes and proteins.

MATERIALS AND METHODS

Media and Culture Conditions for Human Foreskin-Derived MSCs

hMSCs were cultured either in culture medium consisting of Dulbecco Modified Eagle Medium +4.5 g/L glucose, + glutamine w/o pyruvate (DMEM; Gibco, Orlando, FL) supplemented with 10% fetal bovine serum (FBS; Gibco), and 1% penicillin/streptomycin solution (P/S; Gibco, Orlando) or in dietary medium, which had the same composition but a lower content of FBS (1%). Cells were maintained in a humidified incubator at 37°C and 5% CO_2.

Isolation and Expansion of Human Mesenchymal Stem Cells (hMSCs)

Procedures were approved by the Ethics Committee of the Ärztekammer Nordrhein, Düsseldorf, and methods were performed according to its guidelines and regulations. Human donors provided their informed consent.

hMSCs were enzymatically isolated from human foreskin biopsies, as described by Ponec et al.[30] Briefly, after removing the epidermis from the dermis, the tissue was cut into small pieces and washed 3 times with phosphate-buffered saline (PBS) at room temperature. Afterward, the pieces were incubated with 0.075% collagenase (500 U/mL; Serva, Heidelberg, Germany) at 37°C under gentle agitation for 12 hours. The enzymatic reaction was stopped by adding DMEM supplemented with 10% FBS (Gibco/Invitrogen).

The suspension was filtered through a 40-μm mesh filter to remove debris and centrifuged at 575*g* for 5 minutes. The cellular pellet was resuspended in DMEM/F-12 with 10% of heat-inactivated FBS and 1% P/S, and cells were plated at a density of 5000 cells/cm^2 onto conventional tissue culture plates (Greiner Bio-One, Frickenhausen, Germany). Culture medium was replaced with fresh medium after 24 hours of cultivation and afterward every 3 to 5 days until the cell layer had reached approximately 80% confluence. Cells were enzymatically passaged at ~80% confluence using 0.05% Trypsin-EDTA (Gibco, South America).

Descemet Peeling of Rabbit Corneas

Rabbit eyes were obtained from a private slaughterhouse "Lapinchen" (Euskirchen, Germany). Rabbit eyes were enucleated, rinsed with PBS to remove blood residuals, and stored in PBS with 10% P/S at 4°C for 4 to 24 hours. The cornea inclusive of a small scleral ring was cut out of the eye and put upside down into manufactured fitting silicone rings. After separating the limbus, the rabbit CE was completely removed by incubation of the posterior cornea with 0.1% EDTA dissolved in osmotic aqua purificata. This procedure was repeated until the rabbit CEC was completely removed.

Seeding of MSCs on Peeled Rabbit Descemet Membrane

Foreskin-derived MSCs (250,000) dispersed in culture medium were seeded on the top of peeled rabbit Descemet membrane, and after 24 hours of incubation, culture medium was exchanged with serum-reduced culture medium. The morphological changes of the MSCs were microscopically examined and photographed daily (Axiover 40 CFL; Zeiss, Göttingen, Germany).

Sighting of Microtopography of Native Rabbit Descemet Membrane

Peeled Descemet membrane was cut into 4 × 4 mm pieces, and topography was investigated with an optical 3D surface measurement system (Alicona; InfiniteFocus, Graz, Austria).

Fabrication of Master molds with 2-Photon Lithography

With 2-photon lithography (2-PL), 4 inverted DLT hexagonal structures with slightly different micro- and nanofeatures were produced (shown as SDC Fig. 1) by polymerizing a resist polymer in a linear manner from outside to inside. As a substrate, a fused silica glass slide was used and coated with OrmoPrime (micro resist technology GmbH) as an adhesion promoter for OrmoComp. For 2-photon polymerization, the commercial device Photonic Professional with a galvo scanner upgrade (Photonic Professional GT; Nanoscribe

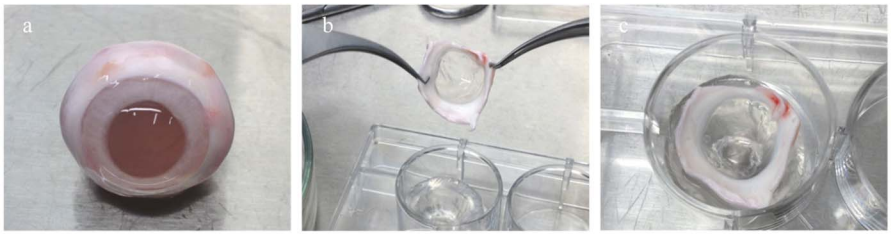

A

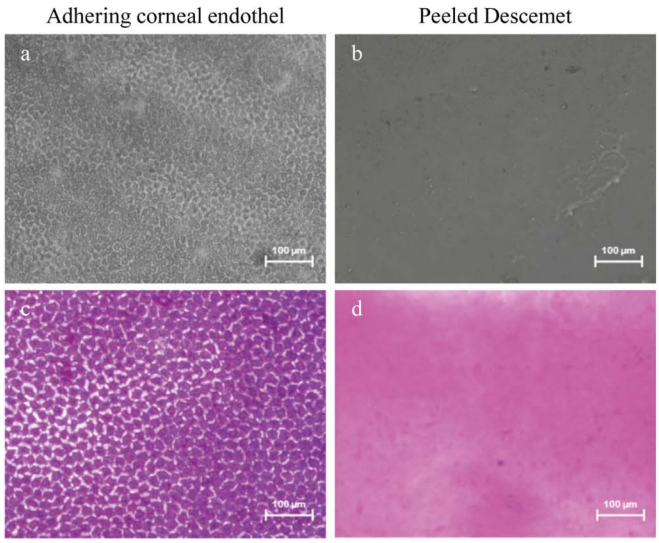

B

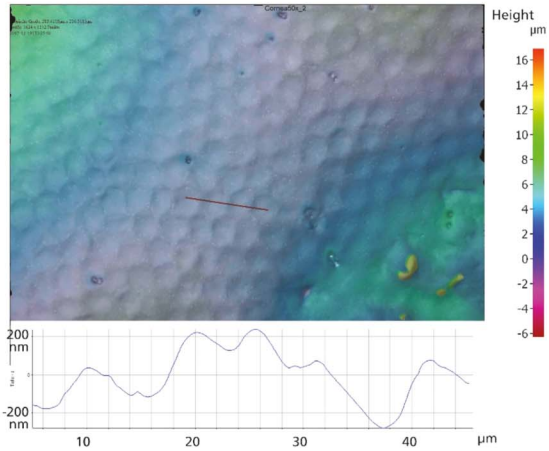

C

FIGURE 1. Detection of rabbit Descemet microtopography and its ability to convert hMSCs into polygonal zonula occludens (ZO-1) and sodium/potassium (Na/K)-ATPase-expressing cells. A, Enucleated rabbit eyes were prepared (a), CECs were completely removed from Descemet membrane (DM). Then, the cornea inclusive of a small sceral ring was cut out of the eye (b) and put upside down into a silicone ring holder (c). B, In comparison to the untreated rabbit cornea (a), peeled DM (b) is free from any CECs. For better visualization, peeled and unpeeled DMs were stained with hemalaun (c, d). C, Surface microtopography of peeled rabbit DM imaged with Alicona microscopy was determined to have a honeycomb pattern. D, hMSCs were cultivated on the control substrate (smooth collagen) (a, b) or on peeled DM (c, d) for 11 days. In contrast to control cells, cultivation on peeled DM induced expression of ZO-1 (c) and Na/K-ATPase (d).

Eggenstein-Leopoldshafen, Germany) was used. The structures were fabricated as shells with a shell thickness of 2 µm. The laser power was varied between 13 and 31 mW, and a writing speed between 800 and 10.400 µm/s was used (see Supplemental Digital Content 1, http://links.lww.com/ICO/A715).

Molding the Descemet-Like Structure in Polydimethylsiloxane (PDMS)

The Descemet-like structure was molded in PDMS; therefore, base and curing agent from Sylgard 184 (Dow Corning) were mixed (mass ratio 10:1) and poured on the template. Liquid PDMS was then degassed by vacuum and afterward cured for 48 hours at room temperature. Flat control pieces were casted from polystyrene petri dishes (Greiner Bio-One). As with the master prints, the corresponding silicone imprints differ in both micrometer and nanometer scales.

Scanning Electron Microscopy of Silicon Substrates

PDMS surfaces were sputter coated with a platinum layer (5 nm) for structural examination by scanning electron microscopy using a Zeiss Neon 40 EsB (SEM; Zeiss, Oberkochen, Germany), equipped with a field emission gun and a thermally assisted Schottky type emitter. Images were taken at an acceleration voltage of 2 keV using an SE detector (Everhart–Thornley detector). Scanning resolution was 2048 × 1536 pixels (see Supplemental Digital Content 1, http://links.lww.com/ICO/A715).

Flow Cytometry

For verifying the multilineage potential of foreskin fibroblast cells of passage 4 were cultivated with DMEM (10% FBS, 1% P/S) in 75 cm^2 tissue culture flasks until 80% confluence had been reached. Cells were stained with surface

marker antibodies against CD105, CD73, and CD90 to detect mesenchymal stemness or against CD14, CD45, CD20, and CD34 to exclude hematopoietic markers, using the manufacturer's protocol (MSC Phenotyping Kit from Miltenyi, Germany). The flow cytometer was compensated for MSCs, and the histogram shift beyond the appropriate isotype control was counted as surface marker–positive cell.

PDMS Surface Treatment and Cell Seeding

Directly before hMSC seeding, PDMS microstructured surfaces were treated with oxygen plasma for sterilization and surface treatment to make it hydrophilic and to enhance cell attachment (plasma device Diener ZEPTO; Ebhausen, Germany). Plasma treatment was performed at 100% power and 0.8 mbar for 60 seconds. MSCs of passage 4 were plated at a density of 900 cells/mm^2 and incubated in a humidified incubator at 37°C and 5% CO_2. After 24 hours of incubation, culture medium was replaced with dietary medium. The morphological changes of the MSCs were microscopically analyzed and photographed daily (Axiover 40 CFL; Zeiss, Göttingen, Germany).

Immunocytochemistry

For immunohistochemical analysis, microstructured PDMS surfaces were carefully washed with PBS. Adherent cells (hMSCs) were fixed with 4% paraformaldehyde (Sigma-Aldrich, Steinheim, Germany) for 20 minutes and then permeabilized with 0.5% Triton-X for 5 minutes (Sigma-Aldrich). After blocking with 10% normal goat serum for 30 minutes, cells were incubated overnight with primary antibodies (Thermo Fisher Scientific) at 4°C in a humidified chamber. Cells were stained for Tight Junction Protein 1 (TJP1, ZO-1) (1:1000) and ATP1A1 (Na/K-ATPase) (1:1000). After washing with 10% normal goat serum, samples stained for TJP1 were incubated with the secondary antibody anti-goat/Mouse-IgG-DyLight-594 (1:1000; Thermo Fisher Scientific) and samples stained for ATP1A1 with anti-goat/Rabbit-IgG-DyLight-488 (1:2000; Thermo Fisher Scientific) for 60 minutes in the dark. Then, cells were washed with PBS, and nuclei were counterstained with DAPI (1:1000 in methanol) for 1 minute. Images were acquired using a Keyence BZ-9000 inverted fluorescence microscope (Keyence, Frankfurt am Main, Germany) and evaluated with BZ-II Analyzer 1.41 software. Specific staining of secondary antibodies was ensured by control stains omitting primary antibodies.

RNA Extraction and cDNA Synthesis

Poly A+ mRNA was extracted from single cells, and cDNA was synthesized using the REPLI-g WTA Single Cell Kit (Qiagen) as per the manufacturer's instructions.

Before that, cell samples were taken and centrifuged at 300*g* for 5 minutes. Supernatant was carefully removed, and the cell pellet was washed with PBS. The centrifugation step was repeated at 300*g* for 5 minutes, and the supernatant was discarded. Seven microliters of H_2O and 4 μL of lysis buffer were added to the cell pellet, which was then stored at −80°C.

Quantitative Real-Time Polymerase Chain Reaction (PCR)

Quantitative real-time PCR was performed using Taqman probe-based technology (Applied Biosystems) for Na/K-ATPase, ZO-1, Col8A2, PITX2, and the commonly used housekeeping gene glyceraldehyde 3-phosphate dehydrogenase (GAPDH). For each gene, a master mix of 10 μL TaqMan GTXpress Master Mix, 7 μL H_2O for injection, and 1 μL TaqMan Gene Expression Assay was prepared. Eighteen microliters of master mix was pipetted into each well of a 96-well plate. Two microliters of cDNA sample (1:100) was then added to each corresponding well. A negative control without cDNA template was run for each gene. All reactions were performed in triplicate. The PCR reaction was performed with the PCR cycler CFX96 (Biorad) under the following conditions: 50°C for 2 minutes, 95°C for 10 minutes, followed by 40 cycles of 95°C for 15 seconds, and 60°C for 1 minute with a plate read at the end of each cycle. Results were normalized to GAPDH and analyzed using the ΔΔCT method.

RESULTS

Decellularization of Native Descemet Membrane

To ensure that Descemet membrane contains a distinctive microtopography, we first had to remove the endothelial cells from rabbit corneas completely, without disturbing the surface (Fig. 1A). The only way to detach the strongly adherent rabbit CECs was to burst the cells with osmotic pressure. As shown in Figures 1Bb–Bd, the rabbit CECs were completely removed.

Imaging of Descemet Microtopography

The topography of peeled Descemet membrane was imaged with 3D confocal microscopy (Alicona, infinite focus) (Fig. 1C). The microtopography consisted of flat hexagonal pits with a maximal web height of 1 μm and a width ranging between 10 and 20 μm. The unique hexagonal combs were irregularly shaped and exhibited a sinusoidal cross section.

Interaction of hMSCs With Various Artificial Descemet Membrane Micro-Like Topographies

With 2-photon lithography (2-PL), 4 inverted DLT hexagonal structures with slightly different micro- and nanofeatures were produced by polymerizing a resist polymer in a linear manner from outside to inside. Just as the master prints, the corresponding silicone imprints differed in both micrometer and nanometer scales. The topography of the 4 different imprints was analyzed with atomic force measurement and had the same width of 16.3 μm but differed in feature depth, ranging between 1.52 and 2.02 μm. The shape included 185 nm steps that varied in deep from 20 to 116 nm (see Supplemental Digital Content 1, http://links.lww.com/ICO/A715). Repeated experiments demonstrated that structure 1 induced the most reliable polygonal cell morphology and

2D cell agglomerate profiles for $CD73^+$, $CD90^+$, $CD105^+$ positive and $CD14^-$, $CD20^-$, $CD34^-$, $CD45^-$ negative hMSCs (data not shown), and thus, further studies were focused on structure 1.

Interaction of hMSCs on Structure 1 Induced Rounding of Cell Cytoplasm and Nuclei

It is well known that the cell cytoplasm and nucleus shape have a strong impact on cell fate. Figure 2A clearly demonstrates that structure 1 induced shrinkage, a polygonal shape (Fig. 2Ab), and accumulation of the cells but also a rounding of the nuclei (Fig. 2Af). In contrast, control cells maintained a typical fibroblastic morphology and oval nuclei (Figs. 2Aa, Ac, Ae).

Formation of Cell Associations

A commonly observed phenomenon was development of elongated cells in a line. These cell types were always located beside islets consisting of hexagonal-shaped cells. To confirm the assumption that these spindle-formed cells were related to the hexagonal-shaped cells, CEC typical marker expression of ZO-1 and Na/K-ATPase was analyzed and confirmed with immunofluorescence staining (Fig. 2B).

Detachment of Islets With Correctly Shaped Hexagonal Cells

The above-described islets with polygonal-shaped cells were found to detach from the PDMS surface (Fig. 2C).

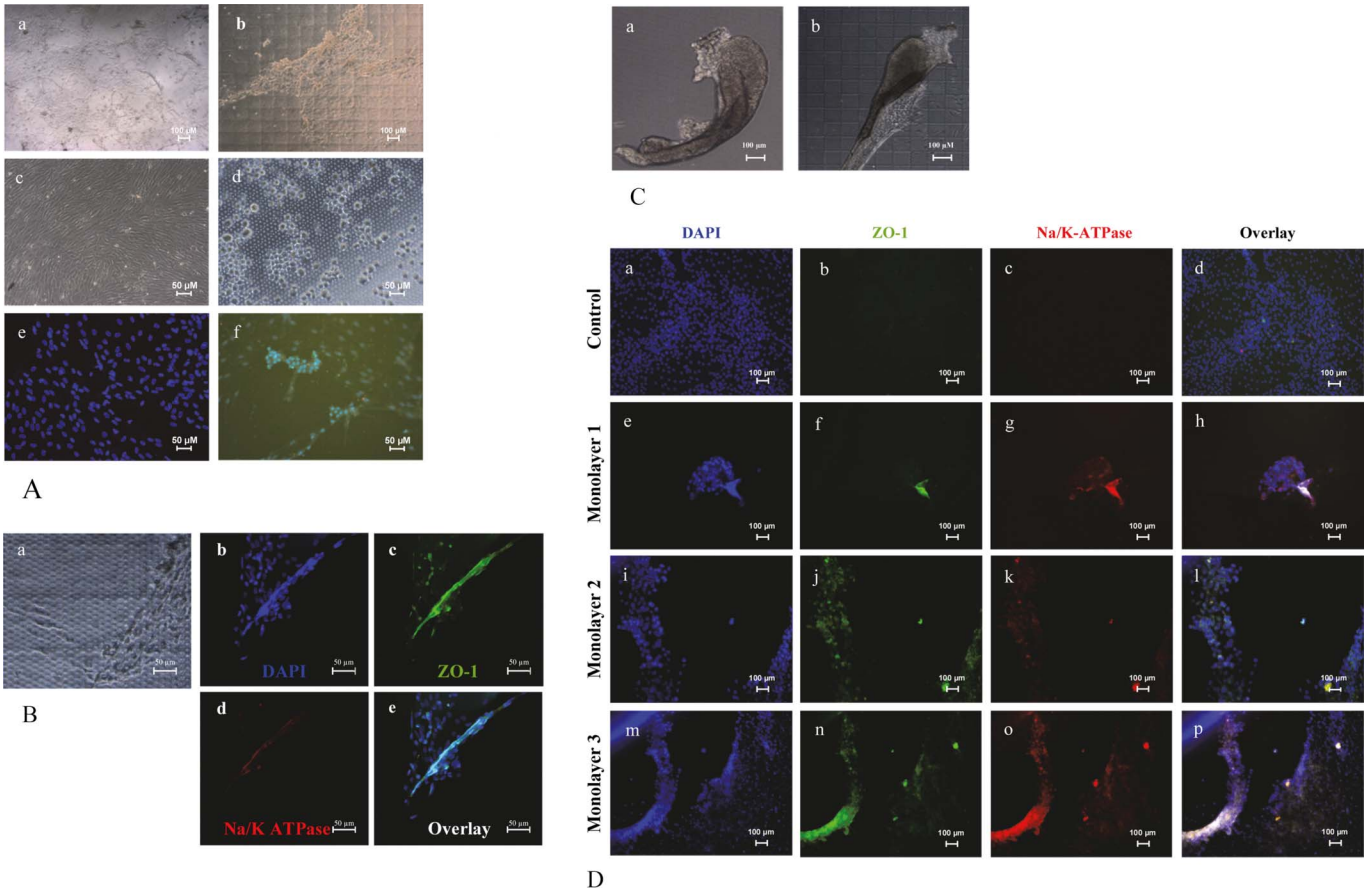

FIGURE 2. Cultivation of hMSCs on structure 1 induced morphological changes and finally detachment of cell monolayer like constructs expressing zonula occludens 1 (ZO-1) and sodium/potassium (Na/K)-ATPase. A, hMSCs were cultivated either on smooth silicone (control, a) or on Descemet-like topography (DLT) 1 for 6 days (b). Bright field microscopy pictures (a–d) showed fibroblastic-shaped control cells (smooth silicone) (a, c) and that hMSCs cultured on structure 1 (S1) (b, d) adapted polygonal morphology and allowing the contact with up to 6 neighboring cells around. Fluorescence microscopy images of DAPI-stained samples (e, f) show round-shaped nuclei of cells cultivated on structure 1 (f) in contrast to oval-shaped nuclei of control cells (e). B, hMSCs cultivated on structure 1 changed their morphology into spindle-like shape (a). The cells were stained with DAPI (b). Immunofluorescence analysis revealed that these constructs stained positive with anti-ZO-1 (c) and anti-Na/K-ATPase (d). The overlay of DAPI, Zo-1, and Na/K-ATPase is shown in (e). C, hMSCs cultivated on structure 1 built up single-layer cell associations and peeled off the surface after 10–14 days of incubation. (a) and (b) show two different monolayers. D, hMSCs were cultured on smooth silicone (a–d) as a control and on DLT 1 (e–p) for 14 days. The cells were stained with 4′,6-Diamidino-2-phenylindole (DAPI) (a, c, i, m), anti-ZO-1 (b, f, j, n), or anti-Na/K-ATPase (c, g, k, o). The 3 single-layer cell associations of hMSCs cultured on DLT1 showed upregulation of ZO-1 (f, j, n) and Na/K-ATPase (g, k, o) compared with control cells (b, c). The overlay of DAPI, Zo-1, and Na/K-ATPase is shown in d, h, l, and p.

Figures 2De–Dp show that cell islets of 3 replicates expressed both ZO-1 and Na/K-ATPase. In contrast, control cells did not detach or express ZO-1 or Na/K-ATPase (Figs. 2Da–Dd).

Changes in Gene Expression due to Cell Density Effects

Furthermore, we analyzed changes of gene expression for ZO-1, ATPase, Col-8, and PITX at different time points, that is, 24 hours and 24 days. First, we analyzed the effect of cell seeding density on CEC differentiation. RNA was extracted and reversed transcribed from cells cultivated on smooth silicone in a concentration of 5000 cells/cm^2 or 3000 cells/mm^2. After 24 hours of cultivation, differences in gene expression between high and low seeding densities were observed with an average of 4.8-fold ZO-1 and 11.7-fold ATPase. The high SD indicated that the cell population was extremely diverse after this short incubation time (Fig. 3Aa). In fact, the SD for Na/K-ATPase and ZO-1 was lower at 24 days, and upregulation of the eye development marker PITX and the basement membrane specific marker Col-8 was observed compared with 24 hours. Specifically, expression of PITX was 2.9-fold and Col-8 was 3.5-fold upregulated, whereas expression of ZO-1 and Na/K-ATPase stabilized at 3.0-fold and 1.7-fold (Fig. 3Ab). Because the high seeding density of 3000 cell/mm^2 alone induced early upregulation of ZO-1 and Na/K-ATPase in a few cells, this seeding density was used in all following experiments.

Combined Effect of Native CE Appropriate Cell Concentration and Descemet Topography

As shown in Figure 3Ba, adhesion to the DLT only marginally enhanced gene expression of ZO-1 up to 1.6-fold and Na/K-ATPase up to 1.8-fold after 24 hours compared with the smooth silicone control. These data confirm the observation that only a few hMSCs seemed to align to the DLT structure after 24 hours. In contrast, after 24 days, the DLT effect on the differentiation process was

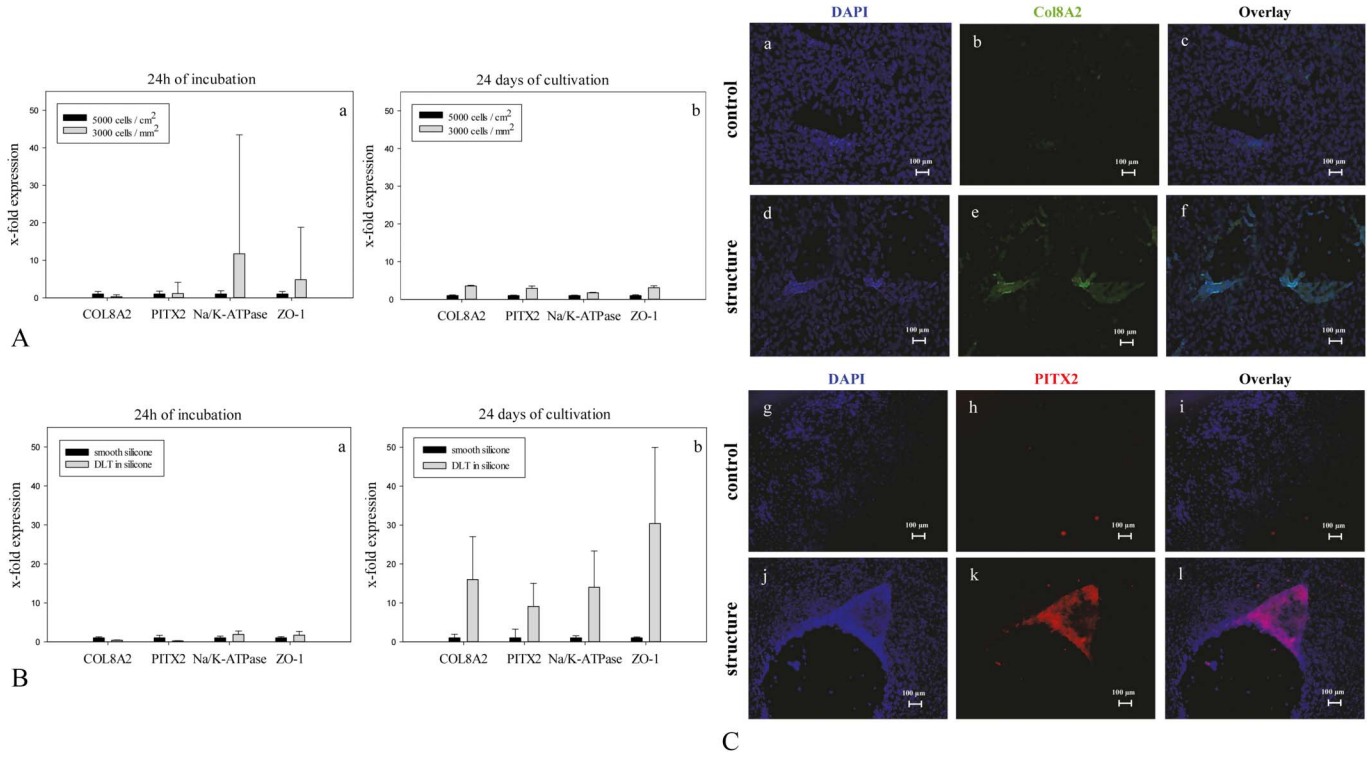

FIGURE 3. Effect of high cell density on expression of human corneal endothelial typical genes as paired-like homeodomain (PITX), collagen 8 (Col8), zonula occludens 1 (ZO-1), and sodium/potassium (Na/K)-ATPase and the impact of the Descemet-like topography (DLT) to differentiate high-density seeded hMSC into corneal endothelial-like cells. A, hMSCs were incubated at a concentration of 5000 cells/cm^2 or 3000 cells/mm^2 on smooth silicone for 24 hours or 24 days. qRT-PCR was performed, and the gene expression levels of ZO-1, Na/K-ATPase, Col8A2, and PITX were compared. Expression was normalized to beta-2 microglobulin (B2M) and polymerase (Pol) R2A or glyceraldehyde 3-phosphate dehydrogenase (GAPDH). An example of the data is presented. B, hMSCs were incubated at a concentration of 3000 cells/mm^2 on smooth (control) or S1 structured silicone for 24 hours or 24 days. Increased expression of ZO-1, Na/K-ATPase, Col8A2, and PITX were observed after cultivation on DLT1 compared with control cells. Expression levels were normalized to that of MHC class I polypeptide-related sequence A (MICA) and PolR2A. C, hMSCs were cultured on smooth or S1 structured silicone for 14 days. The cells were stained with DAPI (a, d, g, j), anti-Col-8 (b, e), or anti-PITX (h, k). Immunofluorescence analysis revealed that DLT induced Col-8 (e) and PITX (k) expression. Figure C c and f demonstrate the overlay of DAPI and Col 8 of Control and Structure and Figure C i and l demonstrate the overlay of DAPI and PITX of Control and Structure. Control cells minimally expressed Col-8 (b) but no PITX (h).

clearly visible, and increased gene expression of ZO-1 and Na/K-ATPase up to 30- and 13-fold, respectively, and of Col-8 and PITX up to 16- and 9-fold, respectively, was found (Fig. 3Bb).

Immunofluorescence Analysis to Confirm Late Expression of PITX and Col-8

To further confirm late expression of PITX and Col-8, hMSCs were cultivated on DLT structured silicone for 24 days. Cells cultivated on the DLT silicone surface considerably expressed Col8A2 (Fig. 3Ce) and PITX (Fig. 3Ck) in contrast to control cells, which expressed both marker proteins only marginally (Fig. 3Cb and Fig. 3Ch).

Impact of Descemet Substrate Stiffness Combined With Native CE-Specific Cell Concentration on Corneal Differentiation Events

Furthermore, we tested the additional impact of a biomaterial with a stiffness comparable to that of native Descemet membrane. To this purpose, hMSCs were seeded onto smooth collagen or onto previously used smooth silicone

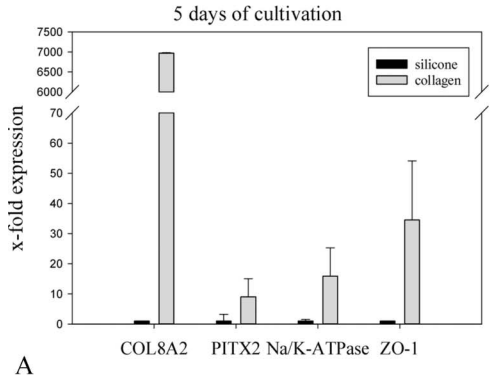

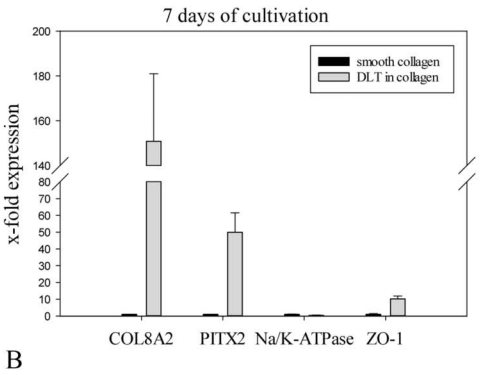

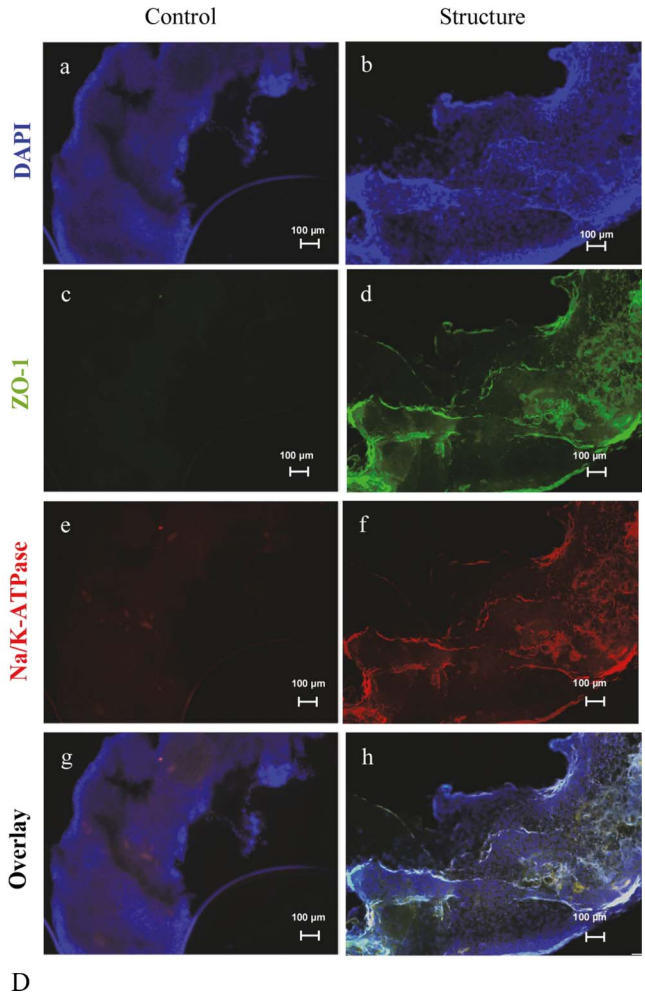

FIGURE 4. Impact of biomimetic collagen to enhance expression of corneal endothelial cell (CEC)-typical markers. A, hMSCs were incubated at a seeding density of 3000 cells/mm^2 on smooth silicone or on smooth collagen for 5 days. Quantitative real-time polymerase chain reaction (qRT-PCR) was performed. Gene expression of zonula occludens 1 (ZO-1), sodium/potassium (Na/K)-ATPase, collagen 8 (Col-8), and paired-like homeodomain (PITX) was clearly increased after cultivation on smooth collagen as compared to smooth silicone. Expression levels were normalized to those of glyceraldehyde 3-phosphate dehydrogenase (GAPDH). B, hMSCs were incubated at a seeding density of 3000 cells/mm^2 on smooth or DLT1 structured collagen for 7 days. Gene expression of ZO-1, Col-8, and PITX was clearly increased after cultivation on Descemet-like topography (DLT1) collagen as compared to smooth collagen. Expression levels were normalized to those of GAPDH. C, hMSCs were cultured on smooth or DLT structured collagen for 14 days. Cells were stained with DAPI (a, b), anti-ZO-1 (c, d), and anti-Na/K-ATPase (e, f). Immunofluorescence analysis revealed that DLT induced ZO-1 (D) and Na/K-ATPase (f) expression. Control cells (c, e) expressed also both markers to a minor degree. The overlay of Dapi and ZO-1 or Na/K-ATPase is shown in g and h.

(control). Cultivation on collagen enhanced expression of Col-8 up to 6971-fold, of PITX up to 9-fold, of ATPase up to 15-fold, and of ZO-1 up to 34-fold compared with control cells cultured on silicone (Fig. 4A).

Combinatorial Effect of Native CE Appropriate Cell Concentration and Descemet Substrate Stiffness and Topography

Moreover, we investigated the combined induction effect of the native CEC concentration with DLT and substrate stiffness. To this aim, structure 1 was molded from the master template into collagen and used as a substrate. After 7 days of cultivation (Fig. 4B), a 150-fold increased expression was observed for Col-8, 50-fold for PITX, and 10-fold for ZO-1. Expression of Na/K-ATPase was in comparison to smooth collagen (control) slightly decreased.

Impact of the Descemet Membrane–Like Structure Molded in Soft Collagen

We also used the DLT embossed collagen to further analyze ZO-1 and Na/K-ATPase protein expression of hMSCs after 7 days of cultivation. Because enhanced gene expression of both genes was visible through the substrate comparison between collagen and silicone (Fig. 4A), we assumed that ZO-1 and Na/K-ATPase were also strongly expressed in the DLT embossed collagen, although it was not visible on gene level (Fig. 4B) after 7 days of cultivation. Explicit protein expression is presented in Figure 4C. These data confirm the assumption that the genes are upregulated but through normalization with control substrate not detectable. In addition, the immunofluorescence analysis further confirmed that both collagen substrates with or without DLT were potent Na/K or ZO-1 inducers for hMSCs, although DLT embossing was much more effective.

DISCUSSION

Descemet membrane as a basement membrane can be regarded as a specialized cell associated network of extracellular matrix that underlies the CECs and significantly contributes to the developmental and tissue maintaining processes.[31] In vitro cultured primary human CECs are entirely dependent on a Descemet similar substrate as they undergo endothelial to mesenchymal transition to a fibroblastic phenotype and lose their functions when cultured on traditional cell culture consumables.[32]

Recently, Pachelsko et al[33] demonstrated that a biomimetic substrate presenting native basement membrane extracellular matrix proteins and mechanical environment may be a key element in bioengineering functional CE layers for potential therapeutic applications. Although this approach might be a milestone as alternative therapy to conventional allograft surgery, the use of donor CECs could not be circumvented. In this study, we could show that human adult MSCs are possibly able to replace donor CECs as a first step toward development of bioartificial grafts with autologous MSC-derived CE-like cells. Taking into account that MSCs can differentiate into specific cell types in vitro and in vivo[34] and have a tendency to acquire tissue specific characteristics when cocultured with specialized cell types or exposed to tissue extracts in vitro,[35] we were not surprised that MSCs adapted a CEC similar phenotype when incubated on peeled rabbit Descemet membrane. To further elucidate exclusively the impact of topography independent of Descemet stiffness and biochemical composition, we produced with 2-PL 4 slightly different negatives from the original Descemet membrane and embossed them into silicone.

Adhesion of hMSCs on each individual structure led to completely different cell responses in both the morphology of single cells and the manner of cell association formations. These observations are congruous with the knowledge that differences of physical cues in the form of both microscale and nanoscale topographical structures have been shown to affect various cell responses including migration, proliferation, endocytosis, and differentiation.[36] Although we have not elucidated if this particular microtopography or nanotopography, or a combination of both, is responsible for any specific cell adhesion protein alignment and response, we could define structure 1 as a reliable tool to change the fibroblastic morphology of hMSCs into a polygonal shape and to cause them to cluster laterally with 6 or more neighboring cells. Surprisingly, we observed that adhesion to DLT embossed in silicone alone not only induced morphological changes and condensation of cells into a coherent cell layer but also enhanced gene expression of ZO-1 and Na/K-ATPase. We postulate that morphological and thereby cytoskeletal changes cause noticeable alteration of the nucleus shape of hMSCs cultivated on DLT and may support the theory of Dahl et al 2007[37,38] that morphological changes of the nuclei allow transcription of other gene regions.

Another observed phenomenon was that the 2D cell layer preceded always from string-like aggregates and led us to speculate that these elongated cells are in an earlier developmental stage. However, we could at least confirm that a relationship exists between the sickle-shaped cell constructions and the finished 2D cell layer because both putative precursor cells and finalized 2D constructs strongly expressed both CEC typical markers ZO-1 and Na/K-ATPase also on protein level.

Moreover, with the background knowledge that the cell number of 3000 cells/mm^2 matches the CEC density of newborn and pediatric human Descemet membrane, we demonstrated that a seeding density of 3000 cells/mm^2 itself induced differentiation of hMSCs into CEC-like cells as short cultivation times elicited ZO-1 and Na/K-ATPase gene expression and long cultivation times enhanced even expression of PITX and Col8A2. Although expression was weak, it was nevertheless a remarkable result considering that PITX is a protein that is expressed during early eye development and initiates subsequent development of the posterior corneal region,[39] whereas Col-8 is expressed at the embryonic stage to build up underlying Descemet membrane.[40] We further tested whether hMSCs seeded densely at 3000 cells/mm^2 and connected laterally to each other were still able to recognize the underlying DLT topography. We observed strong upregulation of all measured CEC typical genes and concluded

that lateral binding of hMSCs did not impair adhesion to the bottom substrate and its topographic information. The large SDs observed in this experiment suggest that only a certain percentage of the cells had been empowered to strongly express all the 4 measured CEC typical markers.

These promising results motivated us to further simulate the native conditions of the in vivo CEC environment with respect to substrate stiffness because it is also known to be a strong mechanotransductive tool to tune the MSC fate.[41] Because on 2D level both effects of topography and stiffness do not interfere with each other,[42] we combined both Descemet membrane stiffness with the promising topography by molding structure 1 in collagen. Initially, when we explored the material effect, we were impressed that in contrast to silicone, adhesion of 3000 hMSCs/mm^2 to smooth collagen induced a very strong expression enhancement for Col-8 and a respectable expression enhancement for PITX2, Na/K-ATPase, and ZO-1 after a relatively short incubation time of 5 days. Finally, the additional induction effect of Descemet topography was clearly measurable for Col-8 and PITX2.

Summarizing, we present a promising strategy to differentiate stem cells into corneal endothelial-like cells. In contrast to others, who use liquid differentiation factors to differentiate MSCs, we forewent any factor and used exclusively mechanical forces. In contrast to factor-induced differentiation, mechanical induction achieved not only CEC typical gene and protein expression but also a drastic morphological change into properly shaped hexagonal or rather polygonal cells, which is a precondition for formation of a functional CEC monolayer. The ability of hMSCs to express Col-8 might be a hint that these cells are not only able to substitute lost CEC cells but also able to generate the predominant protein of the basement membrane, in this case the Descemet membrane.

Nevertheless, it has to be remarked that hMSCs are quite a mixed cell population with different plasticity and lineage direction properties.[43,44] It takes significant skill and a bit of art to reconstruct with these cells the same experimental circumstances, for example, arrangement of the hMSCs after seeding or the portion of more or less plastic cells, which led to strong differences in respect to differentiation effectiveness. In addition, although we used hMSCs originating from foreskin tissue, a cell source with multipotency, we cannot be sure that these cells have the potential to differentiate into fully functional CECs. Nevertheless, with human foreskin–derived MSCs, we chose a cell source of neural crest origin in accordance with naturally derived human CECs.[45,46] Finally, to pursue the objective to generate autologous CECs of each sex and age, the cell source would need to be changed; a good alternative could be endothelial precursor cells from urine.[47]

REFERENCES

1. Dikstein S, Maurice DM. The metabolic basis to the fluid pump in the cornea. *J Physiol.* 1972;221:29–41.
2. Engelmann K, Bednarz J, Valtink M. Prospects for endothelial transplantation. *Exp Eye Res.* 2004;78:573–578.
3. Joyce NC. Cell cycle status in human corneal endothelium. *Exp Eye Res.* 2005;81:629–638.
4. Tan DT, Dart JK, Holland EJ, et al. Corneal transplantation. *Lancet.* 2012;379:1749–1761.
5. Wu EI, Ritterband DC, Yu G, et al. Graft rejection following descemet stripping automated endothelial keratoplasty: features, risk factors, and outcomes. *Am J Ophthalmol.* 2012;153:949–957.
6. Price MO, Gorovoy M, Price FW, et al. Descemet's stripping automated endothelial keratoplasty: three-year graft and endothelial cell survival compared with penetrating keratoplasty. *Ophthalmology.* 2013;120:246–251.
7. Zhu YT, Chen HC, Chen SY, et al. Nuclear p120 catenin unlocks mitotic block of contact-inhibited human corneal endothelial monolayers without disrupting adherent junctions. *J Cel Sci.* 2012;125:3636–3648.
8. Peh GS, Toh KP, Wu FY, et al. Cultivation of human corneal endothelial cells isolated from paired donor corneas. *PLoS One.* 2011;6:e28310.
9. Peh GS, Chng Z, Ang, et al. Propagation of human corneal endothelial cells: a novel dual media approach. *Cell Transplant.* 2015;24:287–304.
10. Joyce NC, Zhu CC. Human corneal endothelial cell proliferation: potential for use in regenerative medicine. *Cornea* 2004;23:8–19.
11. Schmitz AA, Govek EE, Bottner B, et al. Rho GTPases: signaling, migration, and invasion. *Exp Cel Res.* 2000;261:1–12.
12. Okumura N, Koizumi N, Ueno M, et al. ROCK inhibitor converts corneal endothelial cells into a phenotype capable of regenerating in vivo endothelial tissue. *Am J Pathol.* 2012;181:268–277.
13. Kimoto M, Shima N, Yamaguchi M, et al. Role of hepatocyte growth factor in promoting the growth of human corneal endothelial cells stimulated by L-ascorbic acid 2-phosphate. *Invest Ophthalmol Vis Sci.* 2012;53:7583–7589.
14. Aboalchamat B, Engelmann K, Bohnke M, et al. Morphological and functional analysis of immortalized human corneal endothelial cells after transplantation. *Exp Eye Res.* 1999;69:547–553.
15. Bednarz J, Teifel M, Friedl P, et al. Immortalization of human corneal endothelial cells using electroporation protocol optimized for human corneal endothelial and human retinal pigment epithelial cells. *Acta ophthalmologica Scand.* 2000;78:130–136.
16. Kinoshita S, Koizumi N, Ueno M. Injection of cultured cells with a ROCK inhibitor for bullous keratopathy. *N Engl J Med.* 2018;378:995–1003.
17. Yokoo S Yamagami S, Yanagi Y, et al. Human corneal endothelial cell precursors isolated by sphere-forming assay. *Invest Ophthalmol Vis Sci.* 2005;46:1626–1631.
18. Amano S, Yamagami S, Mimura T, et al. Corneal stromal and endothelial cell precursors. *Cornea.* 2006;25(10 suppl 1):73–77.
19. Mimura T, Yamagami S, Yokoo S, et al. Selective isolation of young cells from human corneal endothelium by the sphere-forming assay. *Tissue Eng Part C Methods.* 2010;16:803–812.
20. Navaratnam J, Utheim T, Rajasekhar V, et al. Substrates for expansion of corneal endothelial cells towards bioengineering of human corneal endothelium. *J Funct Biomater.* 2015;6:917–945.
21. Zhang K, Pang K, Wu X, et al. Isolation and transplantation of corneal endothelial cell-like cells derived from in-vitro-differentiated human embryonic stem cells. *Stem Cell Dev.* 2014;23:1340–1354.
22. Lee S, Tang C, Cao F, et al. Effects of cell number on teratoma formation by human embryonic stem cells. *Cell Cycle.* 2009;8:2608–2612.
23. Narsinh KH, Wu JC. Gene correction in human embryonic and induced pluripotent stem cells: promises and challenges ahead. *Mol Ther J Am Soc Gene Ther.* 2010;18:1061–1063.
24. Joyce NC, Harris DL, Markov V, et al. Potential of human umbilical cord blood mesenchymal stem cells to heal damaged corneal endothelium. *Mol Vis.* 2012;18:547–564.
25. Shao C, Fu Y, Lu W, et al. Bone marrow-derived endothelial progenitor cells: a promising therapeutic alternative for corneal endothelial dysfunction. *Cells Tissues Organs.* 2011;193:253–263.
26. Hatou S, Yoshida S, Higa K, et al. Functional corneal endothelium derived from corneal stroma stem cells of neural crest origin by retinoic acid and Wnt/beta-catenin signaling. *Stem Cell Dev.* 2013;22:828–839.
27. Ju C, Zhang K, Wu X, et al. Derivation of corneal endothelial cell-like cells from rat neural crest cells in vitro. *PLoS One.* 2012;7:e42378.
28. Chen P, Chen JZ, Shao CY, et al. Treatment with retinoic acid and lens epithelial cell-conditioned medium in vitro directed the differentiation of

pluripotent stem cells towards corneal endothelial cell-like cells. *Exp Ther Med 2015.* 2015;9:351–360.
29. Driscoll TP, Cosgrove BD, Heo S, et al. Cytoskeletal to nuclear strain transfer regulates YAP signaling in mesenchymal stem cells. *Biophysical J.* 2015;108:2783–2793.
30. Ponec M, Weerheim A, Kempenaar J, et al. Lipid composition of cultured human keratinocytes in relation to their differentiation. *J lipid Res*. 1988;29:949–961.
31. Ali M, Raghunathan V, Li JY, et al. Biomechanical relationships between the corneal endothelium and Descemet's membrane. *Exp Eye Res.* 2016;152:57–70.
32. Lee JG, Ko MK, Kay EP. Endothelial mesenchymal transformation mediated by IL-1beta-induced FGF-2 in corneal endothelial cells. *Exp Eye Res.* 2012;95:35–39.
33. Palchesko RN, Lathrop KL, Funderburgh JL, et al. In vitro expansion of corneal endothelial cells on biomimetic substrates. *Scientific Rep.* 2015;5: 7955.
34. Pittenger MF, Mackay AM, Beck SC. Multilineage potential of adult human mesenchymal stem cells. *Science.* 1999;284:143–147.
35. Nombela-Arrieta C, Ritz J, Silberstein LE. The elusive nature and function of mesenchymal stem cells. *Nat Rev Mol Cell Biol.* 2011;12: 126–131.
36. Dalby MJ, Gadegaard N, Tare R, et al. The control of human mesenchymal cell differentiation using nanoscale symmetry and disorder. *Nat Mater.* 2007;6:997–1003.
37. Dahl KN, Ribeiro AJ, Lammerding J. Nuclear shape, mechanics, and mechanotransduction. *Circ Res.* 2008;102:1307–1318.
38. Paluch EK, Nelson CM, Biais N, et al. Mechanotransduction: use the force(s). *BMC Biol.* 2015;13:47.
39. Gage PJ, Kuang C, Zacharias AL, et al. The homeodomain transcription factor PITX2 is required for specifying correct cell fates and establishing angiogenic privilege in the developing cornea. *Dev Dyn.* 2014;243:1391–1400.
40. Hopfer U, Fukai N, Hopfer H, et al. Targeted disruption of Col8a1 and Col8a2 genes in mice leads to anterior segment abnormalities in the eye. *FASEB J.* 2005;19:1232–1244.
41. Engler AJ, Sen S, Sweeney HL, et al. Matrix elasticity directs stem cell lineage specification. *Cell*. 2006;126:677–689.
42. Huebsch N, Arany PR, Mao S, et al. Harnessing traction-mediated manipulation of the cell/matrix interface to control stem-cell fate. *Nat Mater.* 2010;9:518–526.
43. Cai J, Miau X, Li Y, et al. Whole-genome sequencing identifies genetic variances in culture-expanded human mesenchymal stem cells. *Stem Cel Rep.* 2014;3:227–233.
44. De Almeida DC, Ferreira MR, Franzen J, et al. Epigenetic classification of human mesenchymal stromal cells. *Stem Cel Rep.* 2016;6:168–175.
45. Wong CE, Parato C, Dours-Zimmermann MT, et al. Neural crest-derived cells with stem cell features can be traced back to multiple lineages in the adult skin. *J Cel Biol.* 2006;175:1005–1015.
46. Lorenz K, Sticker M, Schmelzer E, et al. Multilineage differentiation potential of human dermal skin-derived fibroblasts. *Exp Dermatol.* 2008; 17:925–932.
47. He W, Zhu W, Cao Q, et al. Generation of mesenchymal-like stem cells from urine in pediatric patients. *Transplant Proc.* 2016;48:2181–2185.